Bioconjugate Chemistry

Article

Cite This: *Bioconjugate Chem.* 2019, 30, 2939−2946

pubs.acs.org/bc

Theranostic Quercetin Nanoparticle for Treatment of Hepatic Fibrosis

Qiang Zhang,[†,#] Dan Xu,[†,#] Qiuyan Guo,[†] Wenjun Shan,[*,§] Jun Yang,[⊥] Tongtong Lin,[†] Shefang Ye,[†] Xi Zhou,[†] Yunlong Ge,[⊥] Shengli Bi,[∥] and Lei Ren[*,†,‡]

[†]Key Laboratory of Biomedical Engineering of Fujian Province University/Research Center of Biomedical Engineering of Xiamen, Department of Biomaterials, College of Materials, Xiamen University, Xiamen 361005, P. R. China

[‡]State Key Lab of Physical Chemistry of Solid Surfaces, Xiamen University, Xiamen 361005, P. R. China

[§]Department of Pharmacology, College of Pharmacy, Army Medical University (Third Military Medical University), Chongqing 400038, P. R. China

[∥]National Institute for Viral Disease Control and Prevention, Chinese Center for Disease Control and Prevention, Beijing 102206, P. R. China

[⊥]Department of Neurosurgery, Xiang'an Hospital of Xiamen University, School of Medicine, Xiamen University, Xiamen 361005, P. R. China

Supporting Information

ABSTRACT: The progression of hepatic fibrosis can lead to cirrhosis and hepatic failure, but the development of antifibrotic drugs have faced the challenges of poor effectiveness and targeted specificity. Herein, a theranostic strategy was carried to encapsulate a natural medicine (Quercetin, QR) into hepatitis B core (HBc) protein nanocages (NCs) for imaging and targeted treatment of hepatic fibrosis. It was noted that nanoparticles (RGD-HBc/QR) with surface-displayed RGD targeting ligand exhibit a rather high selectivity toward activated HSCs via the binding affinity with integrin $\alpha_v\beta_3$, and an efficient inhibition of proliferation and activation of hepatic stellate cells (HSCs) in vitro and in vivo. Once encapsulated in quercetin−gadolinium complex and/or labeled with the NIR fluorescent probes (Cy5.5), the resulting nanoparticles (RGD-HBc/QGd) show great potential as NIR fluorescent and magnetic resonance imaging contrast agents for hepatic fibrosis in vivo. Therefore, the multifunctional integrin-targeted nanoparticles could selectively deliver QR to the activated HSCs, and may provide an effective antifibrotic theranostic strategy.

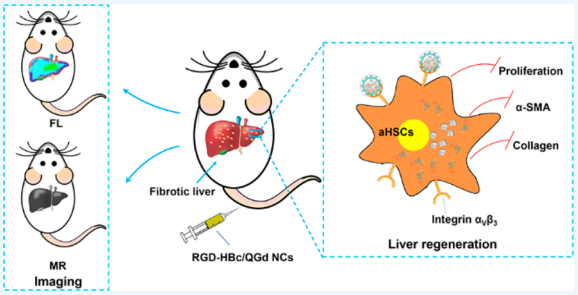

INTRODUCTION

The liver is one of the most important organs that plays a central role in detoxifying and transforming chemicals, which consequently puts the liver in the pathway of exposure to harmful agents and increases its susceptibility to diseases. Over 10% of the world population suffers from liver diseases.[1] Among all liver ailments, fibrosis has emerged as a major health concern. It is the consequence of a sustained wound healing response to a chronic liver injury from a variety of causes including viral, autoimmune, drug induced, cholestatic, and metabolic diseases.[2] Fibrosis can lead to cirrhosis and ultimately to hepatocellular carcinoma and irreversible liver failure.[3]

To date, there is no specific and effective antifibrotic therapy on record, and otherwise varieties of complications are caused by synthetic drugs.[4] Since herbal medicines are now replacing synthetic pharmaceuticals and looked upon as sources of novel bioactive substances, a number of herbal derivatives show promising effects against hepatic fibrosis either experimentally in cell culture (in vitro) and in animals models (in vivo) or even in clinical trials.[5] Quercetin (QR), one of the most abundant natural flavonoids in human diet with no side effects, exhibits various pharmacological properties such as antioxidative and anti-inflammatory activities under pathological circumstances.[6] It was found that quercetin could significantly suppress the activation of the fibroblasts, partly because of its ability to downregulate the NF-κB signal transduction pathway which has critical functions in the regulation of inflammatory responses via multiple mechanisms.[7] It was also found that QR inhibited inflammation induced by carbon tetrachloride (CCl_4) through its antioxidant activity and regulation of TLR2/TLR4 and MAPK/NF-kappa B signal transduction pathways.[8]

Hepatic fibrogenesis is a complex process involving a variety of pathogenic and host-specific signal transduction processes, and it is characterized by immoderate production and

Received: September 19, 2019
Revised: October 21, 2019
Published: October 23, 2019

DOI: 10.1021/acs.bioconjchem.9b00631
Bioconjugate Chem. 2019, 30, 2939−2946

deposition of extracellular matrix (ECM).[9] Activated hepatic stellate cells (aHSCs), portal fibroblasts, and myofibroblasts of bone marrow origin have been identified as the major collagen producing cells.[10] When the liver is damaged by inflammatory, hepatitis viruses, or mechanical processes, hepatic stellate cells (HSCs) can be activated to produce activating cytokines which promote cell proliferation.[11] The aHSCs may promote the proliferation of myofibroblasts and irreversible ECM deposition through paracrine or autocrine mechanisms.[12] Both HSCs activation and their number alteration can result in fibrogenesis. Although the HSCs phenotype is difficult to reverse after activation, reversal is not impossible. Recent studies support the hypothesis that liver fibrosis can be modulated by promoting apoptosis of aHSCs. Considering that the liver is a nonimmunological organ, and engaged primarily in metabolism, nutrient storage, and detoxification, targeting aHSCs has thus become an attractive strategy for treatment of hepatic fibrosis.[13,14] The aHSCs-targeted delivery strategy may not only induce aHSCs apoptosis and increase the antifibrotic action, but also improve the microenvironment, prolong drug release, and reverse drug resistance, and reduce the toxicity. Moreover, it has been found that integrin $\alpha_v\beta_3$ could be expressed by HSCs during their activation, and the expression correlates well with the degree of hepatic fibrosis, which is a specifically biological targets on aHSCs for treatment of hepatic fibrosis.[15,16]

Few of clinic studies have demonstrated a reversal of hepatic fibrosis in early stages, thus early diagnosis is necessary and important for patients to avoid exacerbation and reduce the mortality rate of patients.[17] Despite biopsy is a gold standard for hepatic fibrosis in clinical diagnosis, it is an invasive procedure with a small but significant risk of life-threatening complications.[18] Therefore, it is important to develop a safe, reliable, and noninvasive screening method for precise detection and evaluation of hepatic fibrosis. Magnetic resonance imaging (MRI) is a powerful and important imaging modality in clinical settings because of its highest spatial resolution to soft tissues.[19] Near-infrared fluorescence (NIR FL) bioimaging technology has attracted a great amount of attention due to the deep tissue penetration, low background fluorescence interference, and minimal biological damage.[20] Therefore, dual modal MR/NIR imaging probe could be an attractive combination for precise diagnosis of hepatic fibrosis, which allows full body screening of the probe uptake by MRI and quantification by NIR.

A plethora of nanomaterials has been developed to address some limitations of conventional drug delivery systems, and tried to revolutionize the diagnosis and treatment of several diseases, in particular by selectively directing therapeutic agents to the target tissues and cells.[21] In recent years, a lot of nanomaterials-based medicines have been used to resist variable liver diseases, such as liver cancer,[22] drug-induced hepatic damage,[23] and hepatic ischemia-reperfusion injury.[24] Among the many nanomaterials that are being developed for therapeutic applications, protein nanocages (NCs) are the most powerful and safe carriers, hold unique features including excellent biocompatibility, biodegradation, efficient cell permeability, and suitable pharmacokinetics, which make them highly attractive as ideal drug delivery systems for pharmaceuticals and/or imaging probes.[25] The self-assembling hepatitis B core protein (HBc) NCs are the most flexible protein engineering platforms which caged the structure of both the interior and the exterior, which could be easily engineered though chemical or genetical modifications.[26] HBc NCs are composed of natural biological building blocks, share important features such as facile production, the capacity to cross the biological barrier, as well as the biocompatibility and biodegradability in mammals, which make them excellent choices for targeted drug delivery.[27]

Herein, we report the design of the theranostic QR nanoparticles based on HBc NCs, allowing dual modal (NIR/MR) molecular imaging, and targeted therapy of hepatic fibrosis. To overcome the poor aqueous solubility and bioavailability of QR, the sulfobutylether-β-cyclodextrin (SBE-β-CD) as hydrophobic pockets was introduced through electrostatic interaction inside the protein nanocages (Scheme 1). The self-assembling nanocages with surface-displayed RGD

Scheme 1. (A) Encapsulation of QR/QGd to RGD-HBc NCs through Self-Assembled Process and (B) Theranostic Property of RGD-HBc/QGd NCs: In vivo FL and MR Imaging of Fibrotic Liver (Left) and Liver Regeneration by aHSC Proliferation (Right)

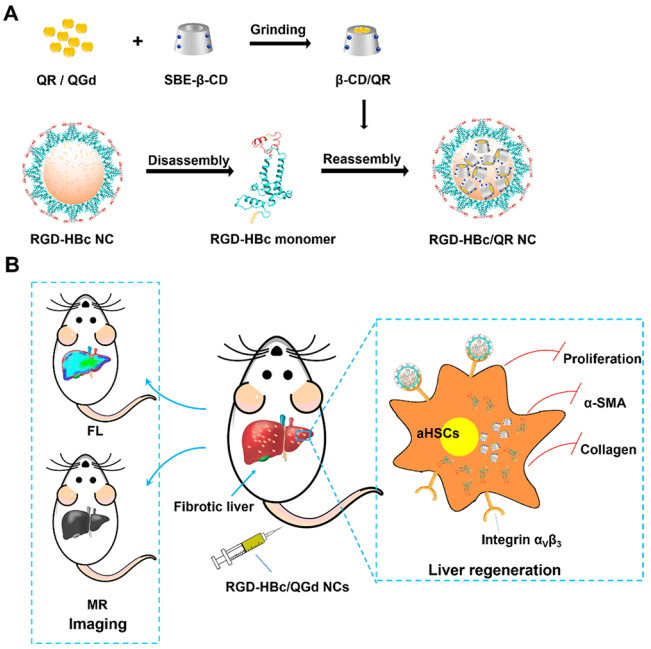

targeting ligands (RGD-HBc/QR) exhibit a rather high selectivity toward activated HSCs via the binding affinity with integrin $\alpha v\beta 3$. It was noted that RGD-HBc/QR NCs exhibit excellent biocompatibilities and specific accumulation in fibrotic livers in CCl_4-induced mice models but not in healthy livers, and efficiently blocking of hepatic fibrogenesis. Once encapsulated quercetin−gadolinium complex (QR-Gd) and/or labeled with the NIR fluorescent probe (Cy5.5), the resulting nanoparticles (RGD-HBc/QGd) exhibited a potential for use as a NIR FL and MR imaging contrast agent for hepatic fibrosis in vivo. The prepared RGD-HBc/QGd realized dual modal imaging and significant antifibrotic effects, therefore it posed a hopeful potential for further biomedical and clinical applications.

RESULTS AND DISCUSSION

Characterization of RGD-HBc/QR and RGD-HBc/QGd NCs. As a member of nature-derived protein nanocage, HBc NCs could be modified easily and precisely through genetic

DOI: 10.1021/acs.bioconjchem.9b00631
Bioconjugate Chem. 2019, 30, 2939−2946

methods, and had been demonstrated to be a flexible nanoplatform for drug delivery. To enhance the affinity with fibrotic liver, the targeting peptide (RGD) was genetically introduced to the major immune region (MIR) of the full length HBc-183 protein between residues 78 and 82 which were fully exposed to the exterior surface. RGD-HBc was expressed in *E. coli*. The SDS-polyacrylamide gel electrophoresis (SDS-PAGE) of purified RGD-HBc protein yielded a single band, which agreed with corresponding to molecular weight of 24 kDa (Figure 1A). Negatively stained transmission

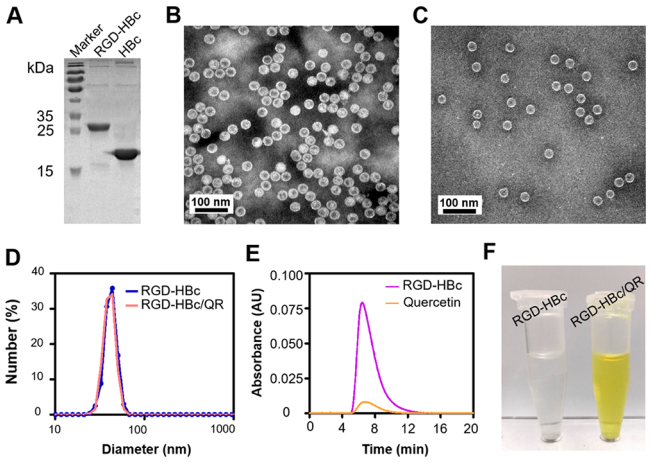

Figure 1. Characterization of RGD-HBc NCs. (A) SDS-PAGE analysis of RGD-HBc NCs and HBc NCs. Representative TEM image of (B) RGD-HBc NCs and (C) RGD-HBc/QR NCS. (D) DLS measurement of RGD-HBc NCs and RGD-HBc/QR NCs. (E) Size exclusion elution profiles of RGD-HBc/QR NCs by HPLC analysis with size-exclusion chromatography (absorbance at 280 and 374 nm). (F) Photograph of RGD-HBc NCs and RGD-HBc/QR NCs.

electron microscopic image (TEM) revealed that the morphology of RGD-HBc NCs were monodispersed and well-defined spheres (Figure 1B), indicating that RGD-HBc proteins could participate in self-assembly.

To effectively load hydrophobic drugs into RGD-HBc NCs, SBE-β-CD was introduced to improve the solubility of QR. The SBE-β-CD possesses high water solubility and negative charge at the outer edge and hydrophobic in the inner cavity, and can be used as envelope of the natural hydrophobic quercetin. The nucleic acid-binding sites of HBc NCs provided positively charged inner cavity, allowing to encapsulate negative charged cargos through the electrostatic interactions. Accordingly, the SBE-β-CD loaded with quercetin could be further encapsulated into the cavities of RGD-HBc NCs in the process of reassembling (Figure S1 of the Supporting Information, SI). Since the complex photodynamical behavior inside the protein and the intermolecular interactions between trapped QR and amino acid residues would affect the absorption spectrum,[28] the blue shift in UV−vis absorption spectra of RGD-HBc/CD/QR NCs means the successful encapsulation of QR by HBc NCs. Through calculations, the loading efficiency of QR in RGD-HBc/CD/QR NCs was 10.09 ± 2.56%, the loading capacity was 16.32 ± 1.75%, and the amount of encapsulated QR was 1996 ± 27 per nanocage. On the basis of the TEM images, a similar morphology of RGD-HBc/QR NCs to that of RGD-HBc NCs was observed (Figure 1C). The average diameter of nanoparticles counted and calculated from the transmission electron microscope (TEM) is 29.6 ± 3.1 nm. Besides, the particle size and the distribution of the RGD-HBc and RGD-HBc/QR NCs were also measured by dynamic light scattering (DLS). The average diameter of the RGD-HBc/QR in water was 32.5 ± 4.1 nm (Figure 1D), which is in good agreement with the diameter of RGD-HBc NCs. As illustrated in Figure 1E, the coelution profiles programmed by high performance liquid chromatography (HPLC) of RGD-HBc NCs (typical absorption peak at 280 nm) and QR (typical absorption peak at 374 nm) after 5 min demonstrated the efficient encapsulation of QR into RGD-HBc NCs. These results revealed that encapsulation of β-CD-QR complex into the cavity of RGD-HBc NCs did not significantly interfere with the self-assembly or alter the cage nanostructure. The photograph of β-CD-QR complex encapsulated RGD-HBc NCs was shown in Figure 1F.

In addition, we also tried to encapsulate the quercetin−gadolinium complex with MRI T_1-enhancing properties into RGD-HBc NCs through SBE-β-CD. RGD-HBc/QGd NCs were further characterized by TEM and DLS. The particle size and morphology of RGD-HBc/QGd NCs were comparable to that of RGD-HBc NCs (Figures S2 and S3).

Previous studies[29] have reported that quercetin−gadolinium complex could be a novel MRI contrast agent. To validate the MRI contrast of RGD-HBc/QGd NCs, the MRI signal in vitro was examined. The typical T_1 weighted spin−echo MRI images recorded for RGD-HBc/QGd NCs at different Gd concentrations in water was shown in Figure 2A. It can be observed

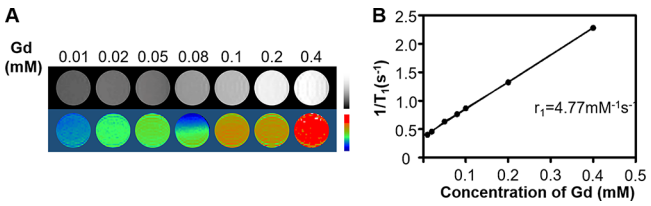

Figure 2. (A) T_1 weighted spin−echo MR images recorded for aqueous solutions of RGD-HBc/QGd NCs with different concentrations of Gd. Images were obtained at 1.5 T (TR/TE 1/4 600/9 ms) at room temperature. (B) T_1 relaxation rate ($1/T_1$) as a function of Gd concentration for RGD-HBc/QGd NCs.

that there was a clearly evident positive contrast enhancement of MRI signals, as demonstrated by the increased brightness. The T_1 relaxivity curves for RGD-HBc/QGd NCs were shown in Figure 2B. The r_1 value of RGD-HBc/QGd NCs was 4.77 mM^{-1} s^{-1}, which was better than commercial T_1 contrast agent Gd-DOTA (r_1 = 3.83 $mM^{-1}\cdot s^{-1}$).[30] These results indicated that NCs could be used as a candidate of T_1 MR imaging contrast agent.

Cytotoxicity and Cellular Uptake. To evaluate the impact of RGD-HBc and RGD-HBc/CD NCs on the viability of HSCs and aHSCs, MTT assay was performed with different concentrations of these carriers after incubation for 24 h, respectively. The cell viabilities in the concentration range from 25 to 300 μg mL^{-1} were more than 80% in both RGD-HBc NCs and RGD-HBc/CD NCs groups (Figure S4). The RGD-HBc and RGD-HBc/CD NCs presumably presented excellent biocompatibility rather than significant cytotoxicity. In fact, this was the groundwork laid for imaging and treatment in vivo, subsequently.

Acetaldehyde has been reported to make HSCs rapidly activate and transdifferentiate to proliferation.[31] Herein, to demonstrate the targeting ability of the RGD-HBc NCs to

DOI: 10.1021/acs.bioconjchem.9b00631
Bioconjugate Chem. 2019, 30, 2939−2946

aHSCs, which were obtained by cocultivation with acetaldehyde in vitro in advance, the cellular internalization process of RGDHBc NCs was carried out. Cy5.5-labeled RGD-HBc NCs were incubated with HSCs and aHSCs for 0.3, 1, 2, and 4 h, respectively. In Figure 3A, the fluorescence signals detected by

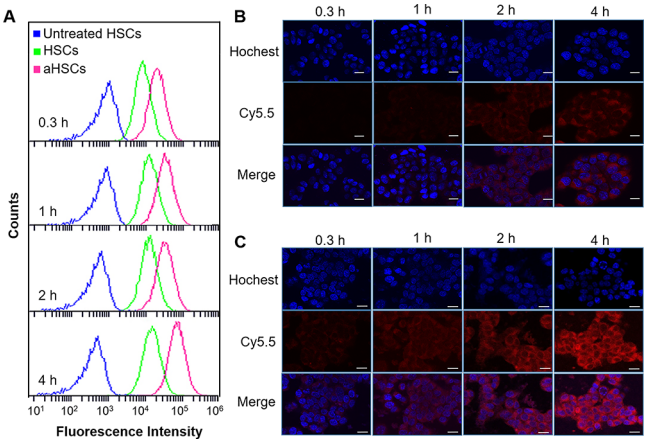

Figure 3. In vitro cellular uptake: HSCs and aHSCs incubated with Cy5.5-labeled RGD-HBc NCs and measured by flow cytometry (A); CLSM of HSCs (B); and aHSCs (C) incubated with Cy5.5-labeled RGD-HBc NCs at the selected time points, respectively. The scale bar is 20 μm.

flow cytometry suggested that RGD-HBc NCs were more prone to be taken up by aHSCs which pretreated with acetaldehyde compared to HSCs without treatment. Moreover, this result could also be confirmed by the results of the confocal laser scanning microscope images (CLSM). As shown in Figure 3B, C, the blue fluorescence was from DAPI-stained cell nuclei while the red fluorescence was from Cy5.5-labeled RGD-HBc NCs. Overall, the merge area indicated that, although the uptake amount was added over time, compared with HSCs cells, the RGD-HBc NCs could bind to the aHSCs faster. On the basis of the fluorescence intensity data of the merge (Figure S5), it was worth noting that the uptake intensity of aHSCs was almost 1.78 times that of HSCs at 4 h. The results thus indicated that RGD peptides, displayed on the surface-exposed spikes of HBc NCs, could promote the cell uptake under recognition of cell surface integrin $\alpha_v\beta_3$ due to the high expression of integrin $\alpha_v\beta_3$ in aHSCs.

In Vitro Antifibrotic Efficacy of RGD-HBc/QR NCs. The state of hepatic stellate cells transferred from quiescent to activated was the central event in the liver fibrosis when the liver damaged. The flavonoid quercetin has displayed anti-inflammatory and antifibrotic effects, and many previous studies have reported that quercetin could inhibit pulmonary fibrosis via preventing activation of HSCs. To evaluate the effect of RGD-HBc/QR NCs on liver fibrosis, cell proliferation, and α smooth muscle actin (α-SMA) expression in HSCs were determined.

A carboxyfluorescein succinimidyl ester (CFSE) proliferation assay was performed to measure cell proliferation. CFSE-labeled aHSCs were incubated with RGD-HBc/QR for 24 h, and then detected the dye dilution by flow cytometry. As shown in Figure 4A, a more robust proliferation of aHSCs was observed, while RGD-HBc/QR-treated aHSCs had 3.3 times and 1.7 times lower proliferation than those of untreated aHSCs and HSCs, respectively (Figure 4B). The results

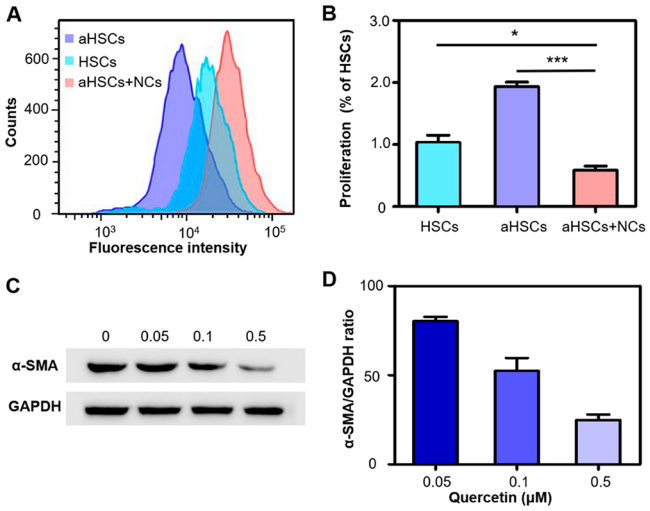

Figure 4. Effects of RGD-HBc/QR NCs on aHSCs in vitro. (A) Representative flow cytometry histograms of CFSE-labeled HSCs, aHSCs, and RGD-HBc/QR NCs-treated aHSCs (aHSCs+NCs) proliferations and (B) the quantitative comparison of the proliferations. (C) Western blot analysis and (D) the quantitative comparison of α-SMA expression in aHSCs cultivated with RGD-HBc/QR NCs at different concentrations of QR (0, 0.5, 0.1, 0.5 μM) for 24 h. The results were normalized relative to expression GAPDH.

suggested that RGD-HBc/QR NCs significantly inhibited proliferation of aHSCs.

The protein expression of α-SMA, which is a special marker of activated HSCs, was detected by Western blotting. As shown in Figure 4C, Western blots results exhibited that RGD-HBc/QR treatment reduced the protein expression of α-SMA. Furthermore, computer assisted semiquantitative analysis (Figure 4D) showed significant dose-dependent decrease in the expression of α-SMA protein. It was noted that RGD-HBc/QR could rapidly and efficiently deliver drugs to targeted cells and inhibit the activation of HSCss.

In Vivo Hepatic Fibrosis Targeting of RGD-HBc/QR NCs. The precise biodistribution of RGD-HBc/QR was evaluated respectively in liver fibrotic mice at the selected time points after intravenous injection of Cy5.5-labeled RGD-HBc/QR NCs. After CCl_4 treatment for 8 weeks, mice could show marked fibrosis in the liver. In Figure 5A, RGD-HBc/QR was rapidly cleared from the blood by the kidney in healthy mice. In contrast, RGD-HBc/QR was significantly accumulated in the fibrotic liver for a relatively long time, which could be associated with the high affinity of RGD-HBc/QR with aHSCs (Figure 5B, C). Besides, the fluorescence signal intensity of ex vivo livers of mice were evidently stronger in the fibrotic group (Figure 5E) than that in the normal group (Figure 5D) at indicated time points (0.3, 2, and 12 h) after intravenous injection. These results suggested that RGD-HBc/QR NCs can be effectively retained in fibrotic livers due to active targeting mediated by RGD.

In Vivo Antifibrotic Efficacy of RGD-HBc/QR NCs. The in vivo activity of RGD-HBc/QR NCs was assessed in the fibrotic group, which was characterized by the obvious fibrosis phenotype from the following analyses. In the fibrotic group, RGD-HBc/QR treatment attenuated the fibrotic level of the fibrotic tissue, the appearance of degenerated hepatocytes, and inflammatory cell infiltration (Figure S5A). Hydroxyproline content is an objective measure of liver fibrosis. The quantification of tissue hydroxyproline (Figure S5B) revealed

DOI: 10.1021/acs.bioconjchem.9b00631
Bioconjugate Chem. 2019, 30, 2939−2946

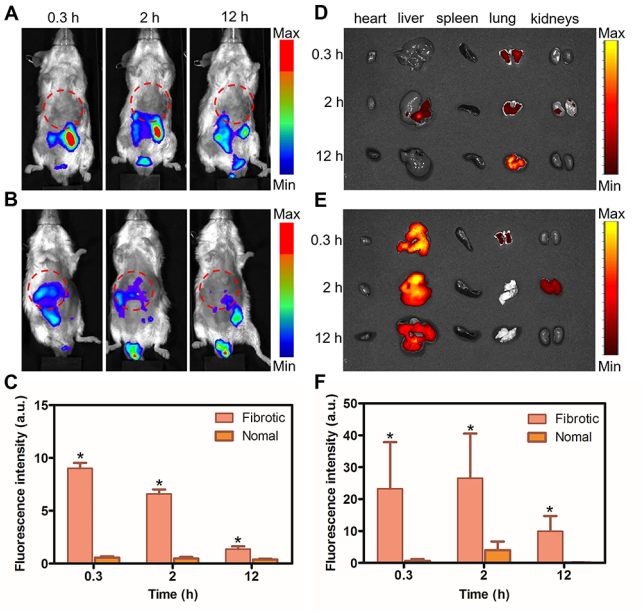

Figure 5. In vivo images of the mice and tissues. The mice in normal group (A) and fibrotic group (B) were i.v. injected with Cy5.5-labeled RGD-HBc NCs. (C) Quantification of the fluorescence intensity in the liver regions (dashed line) of the two groups. The ex vivo images of major organs (heart, liver, spleen, lung, and kidneys) of the mice in normal group (D) and fibrotic group (E) after i.v. injection of Cy5.5-labeled RGD-HBc NCs at selected time points. (F) Quantification of the fluorescence intensity of the ex vivo livers. * $p < 0.05$ compared with normal group.

more than a 1.5-fold reduction for RGD-HBc/QR NCs treated mice compared to fibrotic group. Alanine aminotransferase (ALT) and aspartate aminotransferase (AST) are two of the enzymes central to detect or monitor liver damage. As shown in Figure S5C–E, the enzyme levels of ALT and AST were significantly decreased in the treated group compared to fibrotic group.

The protein levels of α-SMA were measured by immunohistochemistry. As illustrated in Figure 6A, CCl_4 up-regulated the expression of α-SMA, while treatment with RGD-HBc/QR NCs could obviously suppress this increase, from 1.96% ± 0.66% to 1.09% ± 0.33% ($p < 0.05$). Analyses of sirius red stained and masson stained areas, as well as histopathology, also confirmed that RGD-HBc/QR NCs exerted a significantly superior inhibitory effect against activated HSCs (Figure 6B and C). Pathological analysis was performed and is shown in Figure S6, no toxicity was observed in other organs (heart, spleen, lung, and kidneys) of the mice in the three groups (normal, fibrotic, treated) after RGD-HBc/QR NCs injection.

In Vivo Magnetic Resonance (MR) Imaging. To evaluate the efficacy of RGD-HBc/QGd NCs in enhancing MRI contrast in hepatic fibrosis diagnosis and monitor the treatment of RGD-HBc/QR NCs, in vivo MR images were recorded before and after administration of RGD-HBc/QGd with a dose of 0.05 mmol Gd/kg of body weight. Compared with the healthy livers of the normal group (Figure 7A), the fibrotic liver tissues (Figure 7B) appear as a brighter area on the T_1-weighted image at 1 h after injection, indicating that RGD-HBc/QGd NCs could specifically target fibrotic liver, which were consistent with the observations from fluorescence imaging. Since fibrotic livers contain many activated HSCs which express integrin $\alpha_v\beta_3$, RGD-HBc/QGd NCs could accumulate more efficiently than in healthy liver, due to the specific interaction between targeted-ligand RGD and integrin $\alpha_v\beta_3$. Normally, compared with the normal surrounding tissue, fibrotic livers tend to present high RGD-HBc/QGd NCs uptake. Such a difference caused a dramatic signal increase in hepatic lesion and was demonstrated as an optical contrast between fibrosis and normal group tissue on T_1-weighted MR images. In contrast with the normal group, the liver tissues of the treated group appeared hypointense after HBc/QGd NCs injection (Figure 7C), indicating that RGD-HBc/QR NCs treatment had significantly reduced the liver fibrosis. It could also be illustrated by the quantification of MRI in Figure 7D.

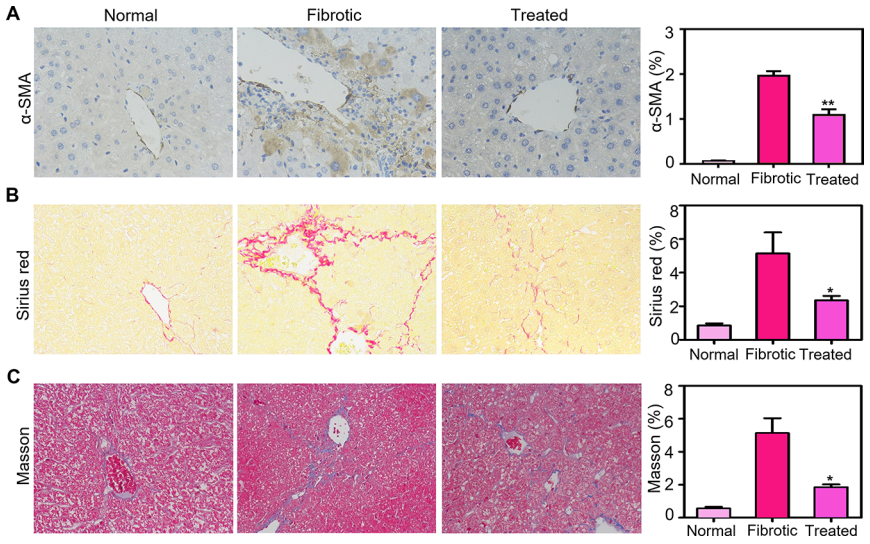

Figure 6. Effects of RGD-HBc/QR NCs on liver fibrosis in the fibrotic group. (A) Liver sections were immunostained for α-SMA to assess HSCs activation. Original magnification, ×400 ($n = 5$). (B) Liver sections were stained with Sirius red to assess collagen deposition. Original magnification, ×400, ($n = 5$). (C) Fibrillar collagen was evaluated by masson staining of liver sections. Original magnification, ×400, ($n = 5$). Masson staining, Sirius red-stained areas, and α-SMA, the areas were analyzed using the Image-pro plus 5.0 software.

DOI: 10.1021/acs.bioconjchem.9b00631
Bioconjugate Chem. 2019, 30, 2939–2946

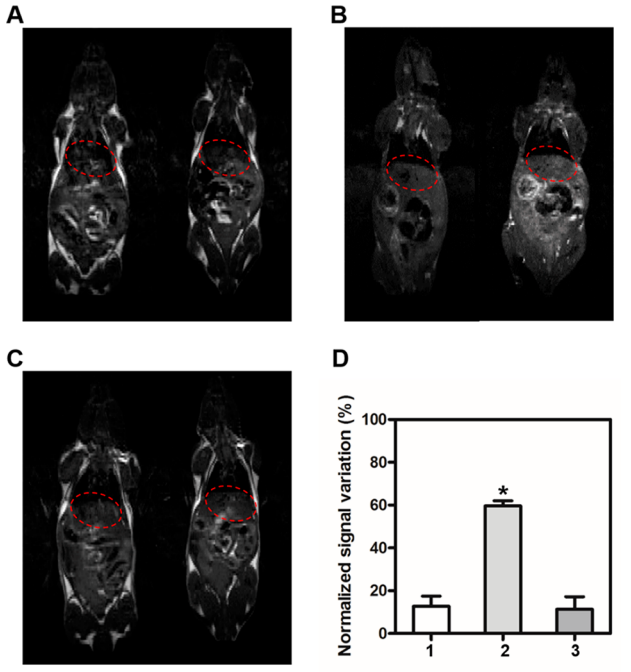

Figure 7. MR images recorded for mice in different groups. Normal liver (A), fibrotic liver (B), and RGD-HBc NCs treated liver (C) at preinjection (left) and 1 h after intravenous injection (right) of RGD-HBc/QGd NCs. The contrast agent was injected at a dose of 0.05 mmol Gd/kg. (D) The quantification of MRI in different groups (1: normal liver; 2: fibrotic liver; and 3: RGD-HBc NCs treated liver). (* $p < 0.05$).

All the results in this section illustrate that RGD-HBc/QGd NCs could not only be used as an MRI contrast agent for fibrosis, but also as a tracer for treatment monitoring.

CONCLUSIONS

In summary, the present study demonstrates that RGD-HBc/QR NCs with excellent biodegradability and biocompatibility can improve the bioavailability of poorly soluble QR, and significantly inhibit hepatic fibrosis. RGD-HBc/QR NCs can be taken up by aHSCs via the binding affinity with integrin $\alpha_v\beta_3$, specifically accumulate in fibrotic liver in CCl_4-induced mice models, and remarkably suppress the activation of HSCs both in vivo and in vitro. Furthermore, RGD-HBc/QR NCs are also a kind of high-performance MR/NIR imaging contrast agent with high T1 relaxivity value and NIR fluorescence through encapsulating Gd contrast agents and labeling NIR-dyes to support noninvasive in vivo evaluation of hepatic fibrosis. Collectively, our work not only develops a potential targeted theranostic agent but also provides a novel strategy for the treatment of fibrotic conditions.

MATERIALS AND METHODS

Preparation and Characterization of the RGD-HBc NCs. The expression and purification of the RGD-HBc NCs were achieved similarly to that described in a previous report.[32] Briefly, the plasmid genetically modified was transformed into an *E. coli* strain, which was expanded and cultured in an LB medium (Sangon Biotech) at 37 °C until the OD 600 nm reached 0.6−0.8. After adding Isopropyl β-D-thiogalactoside (IPTG, 0.1 mM, Aladdin), it was incubated at 17 °C for 18 h. Then, bacteria were collected by centrifugation at 5000 rpm and lysed on ice by sonication. For further purification, DEAE ion-exchange chromatography was carried out after precipitating the suspension with saturated $(NH_4)_2SO_4$ (BBI). At last, the proteins were collected and stored at 4 °C. Molecular weight and purity of protein were analyzed by SDS-PAGE electrophoresis and the morphology of the RGD-HBc NCs was observed by TEM (Tecnai G2 Spirit, FEI, U.S.A.). The size and zeta potential of the RGD-HBc NCs then were measured by DLS (Malvern Zetasizer Nano ZS, Malvern Instruments, Ltd., U.K.).

Synthesis of Quercetin−Gadolinium(III) Complex. The quercetin−gadolinium(III) complex was synthesized following the previous method.[29] Generally, quercetin dihydrate (0.1 M, Sinopharm Chemical Reagent) was dissolved in 25 mL of methanol and 0.1 M of NaOH was added to the solution. Then, a methanol solution (25 mL) dissolved cerium chloride (0.1 M) was slowly added. The mixture solution was stirred at room temperature for about 6 h. The solvent was collected by rotary evaporator and washed with 1:1 chloroform/*n*-butyl alcohol and water to remove the unreacted molecules, followed by vacuum drying overnight to obtain quercetin−gadolinium(III) (QGd) complex.

Drug Packaging. The inclusion complex of SBE-β-CD (Zhiyuan Biotechnology) was prepared by ultrasonication after quercetin (15 mmol) was added into the SBE-β-CD aqueous solution (15 M). The RGD-HBc NCs were incubated in the depolymerization buffer for 1 h, and then the inclusion complex obtained above was loaded into the depolymerized solution and incubated together for another hour. The mixtures were dialyzed in assembling buffer at 4 °C for 24 h (the molecular weight cutoff (MWCO) of dialysis tubing is 3500 Da for the first 12-h, and the MWCO of dialysis tubing is 100 kDa for the second 12-h) to acquire the reassembled nanocages. The drug loading was measured by UV spectrophotometer (UV-2550, Shimadzu, Japan), the morphology and particle size of the nanoparticles packaged with drug were received by TEM and DLS. The amount of encapsulated QR per nanocage was calculated as molar ratio (MR) following the formula below:

$$\mathrm{MR} = (W_{\text{loaded QR}}/M_{\mathrm{QR}})/(W_{\mathrm{NCs}}/M_{\mathrm{NCs}})$$

where $W_{\text{loaded QR}}$ is the mass of the QR encapsulated in RGD-HBc NCs, and W_{QR} is the mass of QR input.

CFSE Proliferation Assay. Hepatic stellate cells were purchased and maintained in DMEM (Hyclone) containing 10% FBS (ABW), 50 unites mL^{-1} penicillin/streptomycin (Hyclone) at 37 °C in a humidified 5% CO_2 atmosphere. Activated HSCs cells were obtained by stimulating HSCs with 200 mM of acetaldehyde for 48 h.[31] HSCs and aHSCs were coincubated with RGD-HBc/QR NCs and collected after removing PBS, CFSE working solution (5 μM working solution in DMEM medium) was added incubating for 10 min. Then half the volume of precooled calf serum was added to stop labeling, standing for 10 min, followed by washing twice with PBS, and resuspension with 1 mL complete medium. Cells were placed on a flow cytometer to measure fluorescence intensity.

Animal Experiments. All animal studies were executed in accordance with IACUC approved procedure at Xiamen University, China (Animal ethics review number: XMU-LAC20160002). Male BABL-c mice (5−6 week, 16−20 g), purchased from Beijing Vital River Laboratories Animal Technology Co., Ltd. by the Laboratory Animal Center of

DOI: 10.1021/acs.bioconjchem.9b00631
Bioconjugate Chem. 2019, 30, 2939−2946

Xiamen University, are free access to standard chow and water. Mice were housed at temperatures of 20−28 °C, relative humidity of 60−70% with ventilation, and 12 h light and dark cycle. Group 1 (n = 5) served as controls and received only pure olive oil. The hepatic fibrosis model was obtained by intervening with CCl_4. Generally, CCl_4 was dissolved in olive oil (1:4), and the mice in group 2 (n = 5) were injected intraperitoneally with 200 μL of CCl_4 solution twice a week for 8 weeks. Group 3 (n = 5) served as the treatment group, in which RGD-HBc/QR NCs were injected via intravenous injection once every 3 days for a month.

In Vivo Fluorescence Imaging. Through in vivo near-infrared fluorescence imaging, the in vivo targeting effect and cycle time of RGD-HBc NCs were visually observed. For oil group mice and CCl_4-treated group mice, 200 μL of RGD-HBc NCs-Cy5.5 was injected through the tail vein and imaged at 0.3, 2, and 12 h. For in vitro imaging, mice were sacrificed at 0.3, 2, and 12 h after injection of RGD-HBc NCs-Cy5.5, and the main organs of heart, liver, spleen, lung, and kidney were observed via the imaging system.

In Vivo MR Imaging. MRI was performed on mice after one month of treatment using 7.0 T Varian MRI system (Agilent Technologies, U.S.A.) with a horizontal-bore Magnex magnet, equipped with 10 cm bore imaging gradients (40 G·cm^{-1}). The testing parameters were adopted: TR (repetition time) = 500 ms, TE (echo time) = 10 ms, slice thickness = 2 mm, FOV = 80 × 50, matrix = 256 × 256. The normal group, the fibrotic group, and the treated group were subjected to isoflurane anesthesia, and T1-weighted imaging images were collected before injection. Thereafter, 100 μL of RGD-HBc/QGd NCs (150 μg mL^{-1}) was injected through the tail vein, and T1 weighted imaging observation was performed at 2 h.

Statistical Analysis. Quantitative data were presented with error bars as mean with SD (standard deviation). Comparisons among groups were determined by one-way ANOVA analysis followed by t test. Differences were considered significant if $p < 0.05$.

■ ASSOCIATED CONTENT

Supporting Information

The Supporting Information is available free of charge on the ACS Publications website at DOI: 10.1021/acs.bioconjchem.9b00631.

Experimental methods such as flow cytometry analysis and blood chemistry, as well as supplementary figures and texts (PDF)

■ AUTHOR INFORMATION

Corresponding Authors

*Phone: +86-236-877163. E-mail: wjshan@tmmu.edu.cn.
*Phone: +86-592-2188530. E-mail: renlei@xmu.edu.cn.

ORCID

Shefang Ye: 0000-0002-9129-7123
Xi Zhou: 0000-0001-5302-5330
Lei Ren: 0000-0003-2131-1601

Author Contributions

#These authors contributed equally.

Notes

The authors declare no competing financial interest.

■ ACKNOWLEDGMENTS

This work was supported by National Natural Science Foundation of China (grants U1505228, U190420008, and 31870994 to L.R.), Science Foundation of Fujian Province (grant 2017Y0078 to L.R.).

■ REFERENCES

(1) Anderson, R. N., and Smith, B. L. (2005) Deaths: leading causes for 2002. *National vital statistics reports 53*, 1−89.
(2) Singh, V., Yeoh, B. S., Chassaing, B., Xiao, X., Saha, P., Aguilera Olvera, R., Lapek, J. D., Zhang, L., Wang, W.-B., Hao, S., et al. (2018) Dysregulated microbial fermentation of soluble fiber induces cholestatic liver cancer. *Cell 175*, 679−694. e22.
(3) Samuel, V. T., and Shulman, G. I. (2018) Nonalcoholic fatty liver disease as a nexus of metabolic and hepatic diseases. *Cell Metab. 27*, 22−41.
(4) Luciano, R. L., and Perazella, M. A. (2014) Nephrotoxic effects of designer drugs: synthetic is not better! *Nat. Rev. Nephrol. 10*, 314.
(5) Li, F.-S., and Weng, J.-K. (2017) Demystifying traditional herbal medicine with modern approach. *Nat. Plants. 3*, 17109.
(6) Luedde, T., and Schwabe, R. F. (2011) NF-κB in the liver—linking injury, fibrosis and hepatocellular carcinoma. *Nat. Rev. Gastroenterol. Hepatol. 8*, 108.
(7) Wu, L., Zhang, Q., Mo, W., Feng, J., Li, S., Li, J., Liu, T., Xu, S., Wang, W., Lu, X., et al. (2017) Quercetin prevents hepatic fibrosis by inhibiting hepatic stellate cell activation and reducing autophagy via the TGF-β1/Smads and PI3K/Akt pathways. *Sci. Rep. 7*, 9289.
(8) Ma, J.-Q., Li, Z., Xie, W.-R., Liu, C.-M., and Liu, S.-S. (2015) Quercetin protects mouse liver against CCl4-induced inflammation by the TLR2/4 and MAPK/NF-κB pathway. *Int. Immunopharmacol. 28*, 531−539.
(9) Schuppan, D., and Afdhal, N. H. (2008) Liver cirrhosis. *Lancet 371*, 838−851.
(10) George, J., Tsuchishima, M., and Tsutsumi, M. (2019) Molecular mechanisms in the pathogenesis of N-nitrosodimethylamine induced hepatic fibrosis. *Cell Death Dis. 10*, 18.
(11) Tsuchida, T., and Friedman, S. L. (2017) Mechanisms of hepatic stellate cell activation. *Nat. Rev. Gastroenterol. Hepatol. 14*, 397.
(12) Wynn, T. A., and Ramalingam, T. R. (2012) Mechanisms of fibrosis: therapeutic translation for fibrotic disease. *Nat. Med. 18*, 1028.
(13) Forbes, S. J., and Newsome, P. N. (2016) Liver regeneration—mechanisms and models to clinical application. *Nat. Rev. Gastroenterol. Hepatol. 13*, 473.
(14) Musso, G., Cassader, M., and Gambino, R. (2016) Non-alcoholic steatohepatitis: emerging molecular targets and therapeutic strategies. *Nat. Rev. Drug Discovery 15*, 249.
(15) Lorenz, L., Axnick, J., Buschmann, T., Henning, C., Urner, S., Fang, S., Nurmi, H., Eichhorst, N., Holtmeier, R., Bódis, K., et al. (2018) Mechanosensing by β1 integrin induces angiocrine signals for liver growth and survival. *Nature 562*, 128.
(16) Rottiers, V., and Näär, A. M. (2012) MicroRNAs in metabolism and metabolic disorders. *Nat. Rev. Mol. Cell Biol. 13*, 239.
(17) Cooper, J., and Giancotti, F. G. (2019) Integrin signaling in Cancer: Mechanotransduction, stemness, epithelial plasticity, and therapeutic resistance. *Cancer Cell 35*, 347−367.
(18) Hamidi, H., and Ivaska, J. (2018) Every step of the way: integrins in cancer progression and metastasis. *Nat. Rev. Cancer 18*, 533.
(19) Heinzmann, K., Carter, L. M., Lewis, J. S., and Aboagye, E. O. (2017) Multiplexed imaging for diagnosis and therapy. *Nat. Biomed. Eng. 1*, 697.
(20) Hong, G., Antaris, A. L., and Dai, H. (2017) Near-infrared fluorophores for biomedical imaging. *Nat. Biomed. Eng. 1*, 0010.
(21) Dehaini, D., Fang, R. H., and Zhang, L. (2016) Biomimetic strategies for targeted nanoparticle delivery. *Bioeng. Transl. Med. 1*, 30−46.

DOI: 10.1021/acs.bioconjchem.9b00631
Bioconjugate Chem. 2019, 30, 2939−2946

(22) Al-Shakarchi, W., Alsuraifi, A., ID, Curtis, A., and Hoskins, C. (2018) Dual Acting Polymeric Nano-Aggregates for Liver Cancer Therapy. *Pharmaceutics 10*, 63.
(23) Amin, K. A., Hashem, K. S., Alshehri, F. S., Awad, S. T., and Hassan, M. S. (2017) Antioxidant and Hepatoprotective Efficiency of Selenium Nanoparticles Against Acetaminophen-Induced Hepatic Damage. *Biol. Trace Elem. Res. 175*, 136.
(24) Ni, D., Wei, H., Chen, W., Bao, Q., Rosenkrans, Z. T., Barnhart, T. E., Ferreira, C. A., Wang, Y., Yao, H., Sun, T., et al. (2019) Ceria Nanoparticles Meet Hepatic Ischemia-Reperfusion Injury: The Perfect Imperfection. *Adv. Mater. 31*, 1902956.
(25) Bhaskar, S., and Lim, S. (2017) Engineering protein nanocages as carriers for biomedical applications. *NPG Asia Mater. 9*, e371.
(26) Whitacre, D. C., Lee, B. O., and Milich, D. R. (2009) Use of hepadnavirus core proteins as vaccine platforms. *Expert Rev. Vaccines 8*, 1565−1573.
(27) Suffian, I. F. B. M., Garcia-Maya, M., Brown, P., Bui, T., Nishimura, Y., Palermo, A. R. B. M. J., Ogino, C., Kondo, A., and Al-Jamal, K. T. (2017) Yield optimization of Hepatitis B virus core particles in E. coli expression system for drug delivery applications. *Sci. Rep. 7*, 43160.
(28) Martin, C., Cohen, B., Gaamoussi, I., Ijjaali, M., and Douhal, A. (2014) Ultrafast dynamics of C30 in solution and within CDs and HSA protein. *J. Phys. Chem. B 118*, 5760−5771.
(29) Muthurajan, T., Rammanohar, P., Rajendran, N. P., Sethuraman, S., and Krishnan, U. M. (2015) Evaluation of a quercetin−gadolinium complex as an efficient positive contrast enhancer for magnetic resonance imaging. *RSC Adv. 5*, 86967−86979.
(30) Bousquet, J.-C., Saini, S., Stark, D., Hahn, P., Nigam, M., Wittenberg, J., and Ferrucci, J., Jr (1988) Gd-DOTA: characterization of a new paramagnetic complex. *Radiology 166*, 693−698.
(31) Page, A., Paoli, P. P., Hill, S. J., Howarth, R., Wu, R., Kweon, S.-M., French, J., White, S., Tsukamoto, H., Mann, D. A., et al. (2015) Alcohol directly stimulates epigenetic modifications in hepatic stellate cells. *J. Hepatol. 62*, 388−397.
(32) Shan, W., Chen, R., Zhang, Q., Zhao, J., Chen, B., Zhou, X., Ye, S., Bi, S., Nie, L., and Ren, L. (2018) Improved Stable Indocyanine Green (ICG)-Mediated Cancer Optotheranostics with Naturalized Hepatitis B Core Particles. *Adv. Mater. 30*, 1707567.

DOI: 10.1021/acs.bioconjchem.9b00631
Bioconjugate Chem. 2019, 30, 2939−2946